A New Global Mode of Earth Deformation: Seasonal Cycle Detected

Geoffrey Blewitt,[1*] David Lavallée,[1] Peter Clarke,[2] Konstantin Nurutdinov[2]

We have detected a global mode of Earth deformation that is predicted by theory. Precise positioning of GPS sites distributed worldwide reveals that in February to March the northern hemisphere compresses (and the southern hemisphere expands), such that sites near the North Pole move downward by 3.0 mm, and sites near the equator are pulled northwards by 1.5 mm. The opposite pattern of deformation occurs in August to September. We identify this pattern as the degree-one spherical harmonic response of an elastic Earth to increased winter loading of soil moisture, snow cover, and atmosphere. Data inversion shows the load moment's trajectory as a great circle traversing the continents, peaking at 6.9×10^{22} kg m near the North Pole in winter, indicating inter-hemispheric mass exchange of $1.0\pm0.2\times10^{16}$ kg.

[1]Nevada Bureau of Mines and Geology, and Seismological Laboratory, University of Nevada, Reno, NV 89557, USA. [2]Department of Geomatics, University of Newcastle, Newcastle upon Tyne, NE1 7RU, UK.

*To whom correspondence should be addressed, E-mail: gblewitt@unr.edu

Redistribution of mass over Earth's surface generates changes in gravitational and surface forces that produces a stress response in the solid Earth, accompanied by characteristic patterns of surface deformation (*1-3*). Here we search for global deformation resulting from Earth's elastic response to a change in the "load moment" (a dipole moment), defined as the load center of mass vector multiplied by the load mass. This predicted degree-one spherical harmonic mode (*1,4*) has unique characteristics that distinguish it from tidal deformation. Our calculations predict that the known seasonal exchange of water and air between the northern and southern hemispheres (*5-7*) is of sufficient magnitude to force such a mode with annual period at the several-millimeter level, which ought to be detectable by modern geodetic techniques. Monitoring this mode should enable global characterization of the hydrological cycle through direct inversion of geodetic data, and enable determination of mechanical properties of Earth on the global scale.

Previous investigations in space geodesy have detected 10-mm level displacement of surface height in response to variation in atmospheric pressure (*8*) and large-scale terrestrial water storage (*9*). Such results show statistically significant correlation between observed site position variations with model predictions. While promising, the residual discrepancies between data and models remain at least as large as the predicted signal. Apart from current uncertainties in modeling ground water storage, another limitation is the level of noise in globally referenced site position data (*9*). We mitigate these problems by seeking a deformation mode with a theoretical functional form (allowing for inversion) and large-scale spatio-temporal coherence (enhancing the signal to noise).

Change in Earth's shape due to the gravitational and pressure stresses of surface loading is theoretically characterized by spherical harmonic potential perturbations and load Love numbers (*2*). Load Love number theory is fundamental to the Green's function approach to loading models (*1*), which has facilitated numerical computation of Earth deformation due to arbitrary load distributions (*3*). Unlike tidal theory, loading theory includes a degree-one deformation generated by movement of the load center of mass with respect to the solid Earth center of mass (*1,4,10*).

Let us define CM as the center of mass of the solid Earth plus the load, and CE as the center of mass of the solid Earth only. CM moves undisturbed in inertial space as the load is redistributed. Conservation of linear momentum requires that redistribution of surface mass displaces CE with respect to CM by the amount (*4*):

$$\Delta\mathbf{r}_{\mathrm{CE}} = -M_{\mathrm{L}}\Delta\bar{\mathbf{r}}_{\mathrm{L}} / M_{\oplus} = -\mathbf{m}/M_{\oplus} \tag{1}$$

where $M_{\oplus} = 6.0\times10^{24}\,\mathrm{kg}$ is Earth system's mass, M_{L} is net mass of load that has been transported over Earth's surface, and $\Delta\bar{\mathbf{r}}_{\mathrm{L}}$ is the change in center of mass of the transported load in the CE frame. We define the "load moment" vector $\mathbf{m} = M_{\mathrm{L}}\Delta\bar{\mathbf{r}}_{\mathrm{L}}$ to emphasize the characteristic of the load that forces this mode of deformation (and to which the data are sensitive). To first order, the displacement of CE creates a tide-raising potential $V_1(\phi,\lambda)$ in the CE frame at latitude ϕ and longitude λ:

$$V_1(\phi,\lambda) = -g\hat{\mathbf{h}}.\Delta\mathbf{r}_{\mathrm{CE}} = g\hat{\mathbf{h}}.\mathbf{m}/M_{\oplus} \tag{2}$$

where $\hat{\mathbf{h}}(\phi,\lambda)$ is the unit vector pointing locally upwards, and g is acceleration due to gravity. Equation (2) is a pure degree-one spherical harmonic function, to which load Love number theory is directly applicable. We assume it is reasonable to ignore the higher degree harmonics because they are orthogonal to the degree-one harmonics, and would not significantly bias the results for a well-distributed global network (*11*). Solutions for surface displacements in the CE frame have been derived in complex spherical harmonic form (*4*), however we have derived solutions in concise vector form:

$$\begin{aligned} \Delta\bar{s}_h &= h_1' V_1 / g = h_1' \hat{\mathbf{h}}.\mathbf{m} / M_{\oplus} \\ \Delta\bar{s}_l &= l_1' \hat{\mathbf{l}}.\nabla V_1 / g = l_1' \hat{\mathbf{l}}.\mathbf{m} / M_{\oplus} \end{aligned} \tag{3}$$

where $\Delta\bar{s}_h$ is upward displacement, $\Delta\bar{s}_l$ is displacement in any lateral direction $\hat{\mathbf{l}}$, and surface gradient operator $\nabla = \hat{\boldsymbol{\varphi}}\partial_\varphi + \hat{\boldsymbol{\lambda}}(1/\cos\phi)\partial_\lambda$. We use load Love numbers modeled by Farrell (*1*), $h_1' = -0.290$ and $l_1' = 0.113$, which are specified in the CE frame.

This global mode of deformation is unique, in that it compresses the hemisphere centered on the load moment, and expands the opposite hemisphere, such that a perfect sphere deforms to another perfect (but strained) sphere of identical diameter. The surface everywhere stretches laterally towards the pole of the load moment. We have discovered that this mode has the peculiar property that there exist reference frames in which the surface deformation field is either purely vertical or purely horizontal. Such an extreme range of equivalent kinematics underscores the need for reference frame consistency when comparing data with models.

Here we use the center of figure frame (CF), defined as having no-net translation with respect to the 3-D surface displacement field. This is an appropriate frame to describe deformations because only relative surface displacement data contribute to the solution, the CE frame is not directly observable, and the CM frame accuracy is limited by model errors in non-gravitational satellite accelerations (*12*). Transformation to the CF frame is accomplished by subtracting from the displacement field the average displacement $\Delta\bar{\mathbf{r}}_{\mathrm{CF}}$ in the CE frame (*4*), which is derived by surface integration of equation (3)

$$\Delta\bar{\mathbf{r}}_{\mathrm{CF}} = \tfrac{1}{3}\left(h_1' + 2l_1'\right)\mathbf{m}/M_{\oplus} \tag{4}$$

where $\Delta\overline{\mathbf{r}}_{\mathrm{CF}}$ is CF variation in the CE frame. The vector form of equation (3) readily allows us to express displacements in the CF frame:

$$\begin{aligned} \Delta\tilde{s}_h &= \Delta\overline{s}_h - \hat{\mathbf{h}}.\Delta\overline{\mathbf{r}}_{\mathrm{CF}} = -\tfrac{2}{3}(l_1' - h_1')\hat{\mathbf{h}}.\mathbf{m}/M_\oplus \\ \Delta\tilde{s}_l &= \Delta\overline{s}_l - \hat{\mathbf{l}}.\Delta\overline{\mathbf{r}}_{\mathrm{CF}} = +\tfrac{1}{3}(l_1' - h_1')\hat{\mathbf{l}}.\mathbf{m}/M_\oplus \end{aligned} \tag{5}$$

Thus, by analogy with equation (2), Farrell's load Love numbers in the CF frame are $\tilde{l}_1' = \frac{1}{3}(l_1' - h_1') = 0.134$ and $\tilde{h}_1' = -2\tilde{l}_1' = -0.268$. Hence, we can express site displacements in the CF frame $\mathbf{\Delta\tilde{s}} = (\Delta\tilde{s}_x, \Delta\tilde{s}_y, \Delta\tilde{s}_z)^{\mathrm{T}}$ by the matrix equation:

$$\mathbf{\Delta\tilde{s}} = \tilde{l}_1' \mathbf{G}^{\mathrm{T}} \mathrm{diag}[+1, +1, -2] \mathbf{G}\, \mathbf{m}/M_\oplus \tag{6}$$

where **G** is the 3×3 matrix that rotates geocentric into topocentric displacements (east, north, and up). Through measurement of site displacements globally, we can invert equation (6) to solve for the components of load moment $\mathbf{m} = (m_x, m_y, m_z)^{\mathrm{T}}$. Alternatively, if the load variation is assumed or known from some independent data source or model, then inverting (6) for the degree one load Love number can test Earth's mechanical properties.

We applied this theory to 5 years of GPS data, acquired by 66 stations of the International GPS Service (IGS) network (*13*). Every week at Newcastle's IGS Global Network Associate Analysis Center, free-network solutions in the CM frame were analyzed to produce site coordinate time series in the CF frame (*14*). The time series were de-trended to remove plate tectonic motion, accounting for correlations between velocity and annual signals (*15*). The resulting time series have a root mean square of ~3 mm (horizontal) and ~7 mm (vertical). Equation (6) was inverted by weighted least squares to solve for the load moment every week.

The load moment results (Fig. 1) show annual oscillations, especially in the z (polar) direction, corresponding to net seasonal mass transport between the northern and southern hemispheres. The maximum downward deformation (Fig. 2) of 3.0 mm points close to the North Pole during February to March, and the South Pole during August to September. Corresponding lateral deformation of 1.5 mm is observed near the equator at these times. The load moment migrates through the year, following the approximate surface trajectory of a great circle (Fig. 3). The maximum load moment is 6.9×10^{22} kg m in the February to March period. The minimum load is observed when it rapidly crosses the equator southwards during May over South America, and northwards during November over Indonesia. We used our load moment time series to produce an empirical seasonal model, estimating amplitudes and phases of annual and semi-annual load moment variations (Table 1, Figs 1 and 3). The annual z component of the load moment peaks at 6.6×10^{22} kg m towards the end of February and August. The empirical seasonal model and equation (6) comprise a predictive calibration model to reduce annual signals in geodetic data (*15*), say for plate tectonics (although more regional effects may dominate individual site time series). The statistics from fitting the time series (Fig. 1) indicate that the precision of our weekly load moment estimates is 3.6×10^{22} kg m (1 standard deviation).

Our results provide constraints on models of mass redistribution. Taking extreme examples, a load moment of 6.6×10^{22} kg m would be produced by net transport of (1) 0.5×10^{16} kg from the South Pole to the North Pole; (2) 1.4×10^{16} kg uniformly distributed from one hemisphere to the other; or (3) 1.1×10^{16} kg from the oceans to land at high latitudes. We suggest that any reasonable model should therefore have a total seasonal transported mass within 40% of 1.0×10^{16} kg. Secondly, models should predict that the load peaks near the poles in their respective late-winter seasons. Thirdly, models should predict that the load's trajectory follows an approximate great circle over the continents (Fig. 3).

From remote sensing it is known that the mass of snow in the northern hemisphere peaks during February to March at 0.3×10^{16} kg (*5, 16*). Recent analysis in atmospheric research (*6*) confirms earlier interpretations (*7*) on the existence of inter-hemispheric oscillations in atmospheric mass at the level of 0.4×10^{16} kg, which appears to be driven in part by anomalous cooling over snow covered areas, particularly over Siberia and Canada (*17*). Our results therefore suggest that the observed pattern of deformation is dominated by winter ground water storage enhanced by atmospheric pressure. Assuming an upper bound on the net redistributed mass at 1.4×10^{16} kg, we infer the non-snow component of winter ground water to be $<0.7\times10^{16}$ kg.

The load's trajectory over the continents (in approximately the y-z plane) is consistent with the land's ability to sustain loads (unlike the ocean's tendency to rapidly approach equilibrium). An interesting feature of the load moment time series is the asymmetric pattern of z oscillations (Fig. 1) and the rapid southward equatorial crossing of mass (Fig. 3) in May. This is consistent with rapid water runoff, which is known to peak during late springtime in the northern hemisphere (*18*). A small y component of load moment also appears during the transition seasons traversing regions of known intense hydrological loading (*9*) in south-east Asia and South America (Fig. 2). An anomaly in the $\pm y$ direction is apparent during 1996/1997, immediately preceding the 1997/1998 El Niño event. Possible mechanisms that might enhance the y component include an equatorial oscillation in (non-steric) sea level across the Pacific (driven by wind stress), and anomalous monsoon precipitation over land.

To conclude, we have detected a global-scale mode of Earth deformation that we have identified as the response of an elastic Earth to redistribution of surface load, specifically the degree one spherical harmonic mode that theoretically corresponds to change in the load moment. This mode compresses one hemisphere, and expands the opposite hemisphere in such a manner that it does not change Earth's overall shape, but nevertheless stretches its surface and so affects site coordinates. In Earth's center of figure frame, the poles appear to be displaced downwards by 3.0 mm during their respective winters, and the equator appears to move towards the winter pole by 1.5 mm. Our novel inversion procedure produces a load moment time series with an annual signal in Earth's polar direction with amplitude 6.6×10^{22} kg m. Stacking reveals the load moment following the approximate trajectory of a great circle traversing the continents, peaking at 6.9×10^{22} kg m near the North Pole in winter. These results are consistent with seasonal loading of land surfaces by fluids, corresponding to an annual mass exchange of $1.0\pm0.2\times10^{16}$ kg between the hemispheres.

References and Notes

1. W. E. Farrell, *Rev. Geophys. and Space Phys.* **10***,* 761, (1972).
2. E. W. Grafarend, J. Engels, P. Varga, *J. Geodesy* **72***,* 11 (1997).
3. T. van Dam, J. M. Wahr, Phys. Chem. Earth **23**, 1077 (1998).
4. A. S. Trupin, M. F. Meier, J. M. Wahr, *Geophys. J. Int.* **108***,* 1 (1992).
5. B. F. Chao, W. P. O'Connor, A. T. C. Chang, D. K. Hall, J. L. Foster, *J. Geophys. Res.* **92**, 9,415 (1987).
6. Z. Guan, T. Yamagata, *Geophys. Res. Lett.* **28***,* 263 (2001).
7. K. Trenberth, *J. Geophys. Res.* **86***,* 5,238 (1981).
8. T. van Dam, G. Blewitt, M. B. Heflin, *J. Geophys. Res.* **99**, 23,939 (1994).
9. T. van Dam *et al., Geophys. Res. Lett.* **28***,* 651 (2001).
10. M. Greff-Lefftz, H. Legros, *Geophys. Journ. Int.* **131**, 699 (1997).
11. For deformations up to degree n, a network can be considered "well-distributed" if neighboring stations everywhere are spaced much less than $180°/n$, which for $n=1$ implies multiple stations in arbitrary hemispheres.
12. J. L. Chen, C. R. Wilson, R. J. Eanes, R. S. Nerem, *J. Geophys. Res.* **104**, 2,683 (1999).
13. Information on relevant GPS station data is provided at www.science.org.
14. P. Davies, G. Blewitt, *J. Geophys. Res.* **105**, 11,083 (2000).
15. G. Blewitt, D. Lavallée, *J. Geophys. Res.*, in press.
16. A. T. C. Chang, J. L. Foster, D. K. Hall, *Rem. Sens. Lett., Int. J. of Rem. Sens.* **11**, 167 (1990).
17. J. Cohen, K. Saito, D. Entekhabi, *Geophys. Res. Lett.* **28**, 299 (2001).
18. Fekete, B.M., C. J. Vörösmarty, W. Grabs, *WMO-Global Runoff Data Centre Rep. 22* (Koblenz, Germany, 1999).
19. We thank J. Wahr and V. Dehant for comments, and IGS for providing data. Supported by DOE grant DE-FC08-98NV12081, NASA grant SENH99-0325-0015, NERC grant GR3/11976, and a UNR International Activities Grant. We thank NSF for supporting continuation of this research.

Table 1 Empirical seasonal load moment model. Amplitude and phases are defined by $A_i \cos[2\pi f_i(t - t_0) - \Phi_i]$ where t_0 is 1 January and f_i is frequency. All parameter values were derived by weighted least squares using the load moment time series (Fig. 1). The 1-standard deviation uncertainties are propagated from scaled coordinate errors (*14*), but do not account for inadequacies of the empirical model, for example, due to inter-annual variability.

	Annual Amplitude A_1 (10^{22} kg m)	Annual Phase Φ_1 (degrees)	Semi-Annual Amplitude A_2 (10^{22} kg m)	Semi-Annual Phase Φ_2 (degrees)
m_x	2.0 ± 0.2	86 ± 3	0.7 ± 0.2	69 ± 13
m_y	2.9 ± 0.2	345 ± 3	0.6 ± 0.2	301 ± 13
m_z	6.6 ± 0.1	56 ± 1	1.5 ± 0.1	207 ± 5

Fig. 1. Estimates of load moment components. Weekly estimates (red) are for (A) x direction towards the intersection of the Greenwich meridian and the equator, (B) y direction, and (C) z direction towards the North Pole. Superimposed is the empirical model (blue) given by Table 1. The weighted root mean square of the time series before/after subtracting the empirical model are (in 10^{22} kg m) 3.9/3.7, 4.2/3.4, and 5.5/2.9, corresponding to square root variance reductions of 1.2, 2.5, and 4.7.

Fig. 2. Observed seasonal variation in Earth deformation. The degree-one surface deformation field uses two-month stacked solutions for (top to bottom) December-January, February-March, April-May, June-July, August-September, and October-November. The left panel refers to vertical deformation, and the right panel to the magnitude of horizontal deformation. Horizontal displacements always point towards the location of maximum downward displacement.

Fig. 3. Trajectory of the load moment as it travels through the year. Each load moment (solid red) is the two-monthly weighted-average of the weekly load moments, stacked over 5 years. The radius of each symbol is proportional to the magnitude. The maximum load moment is 6.9×10^{22} kg m in February-March. The empirical seasonal model (open blue, Table 1) is also plotted for each week.

For www.science.org:

Supplementary Table.

Global GPS station network used for this analysis. A total of 66 stations are listed, with their latitude, longitude, data span analyzed (start date, end date, and span in years), and the percentage of potential data during the span that were collected, analyzed, and accepted. The following criteria were applied to select these stations: (1) at least 104 weekly solutions, (2) analyzed by at least 3 IGS Analysis Centers, (3) time span of at least 2.5 years, and (4) no step functions in the time series related to equipment changes. Finally, a convenient 5-year window of 1996.0 to 2001.0 was selected for the final results, which ensured that no week had a less than 30 contributing stations (see note 11).

Station	Lat	Lon	Start	End	Span	Percent
ALBH	48.390	236.513	1995.872	2001.008	5.14	97
ALGO	45.956	281.929	1995.642	2001.046	5.40	90
AREQ	-16.466	288.507	1995.642	2001.046	5.40	92
ASC1	-7.951	345.588	1996.389	2000.932	4.54	97
AUCK	-36.603	174.834	1996.044	2001.046	5.00	97
BAHR	26.209	50.608	1996.600	2001.046	4.45	90
BOGT	4.640	285.919	1995.661	1999.935	4.27	56
BOR1	52.277	17.073	1995.834	2001.046	5.21	56
BRMU	32.370	295.304	1995.642	2001.046	5.40	97
BRUS	50.798	4.359	1995.910	2000.989	5.08	40
CAS1	-66.283	110.520	1995.661	2001.046	5.39	71
CHAT	-43.956	183.434	1995.949	2001.046	5.10	99
CHUR	58.759	265.911	1996.754	2001.046	4.29	50
CRO1	17.757	295.416	1996.351	2001.046	4.70	85
DAV1	-68.577	77.973	1995.661	2001.046	5.39	78
DGAR	-7.270	72.370	1996.907	2001.046	4.14	96
DRAO	49.323	240.375	1995.642	2001.046	5.40	98
EISL	-27.148	250.617	1995.680	2001.046	5.37	72
FORT	-3.877	321.574	1995.642	2001.046	5.40	98
GALA	-0.743	269.696	1997.789	2001.046	3.26	64
GODE	39.022	283.173	1998.153	2001.046	2.89	96
GOL2	35.425	243.111	1997.290	2001.046	3.76	76
GOLD	35.425	243.111	1995.642	1999.494	3.85	98
GUAM	13.589	144.868	1995.642	2001.046	5.40	95
HOB2	-42.805	147.439	1995.757	2001.046	5.29	84
HRAO	-25.890	27.687	1996.869	2001.046	4.18	65
IISC	13.021	77.570	1995.853	2001.046	5.19	81

IRKT	52.219	104.316	1995.929	2001.046	5.12	94
KELY	66.987	309.055	1996.217	2001.046	4.83	87
KERG	-49.351	70.256	1995.642	2001.046	5.40	90
KIRU	67.857	20.968	1996.217	2001.046	4.83	86
KIT3	39.135	66.885	1995.642	2001.046	5.40	74
KOSG	52.178	5.810	1995.642	2001.046	5.40	97
KOUR	5.252	307.194	1995.642	2001.046	5.40	80
KWJ1	8.722	167.730	1996.447	2001.046	4.60	83
LHAS	29.657	91.104	1995.738	2001.046	5.31	65
MAG0	59.576	150.770	1998.210	2001.046	2.84	95
MAS1	27.764	344.367	1997.233	2001.046	3.81	79
MATE	40.649	16.704	1995.680	2001.046	5.37	85
MDO1	30.681	255.985	1995.872	2001.046	5.17	94
METS	60.217	24.395	1995.699	2001.046	5.35	91
MKEA	19.801	204.544	1996.830	2001.046	4.22	94
NLIB	41.772	268.425	1995.738	2001.046	5.31	81
NTUS	1.346	103.680	1997.693	2000.740	3.05	86
NYA1	78.930	11.865	1998.344	2001.046	2.70	76
NYAL	78.930	11.865	1995.757	2001.046	5.29	79
OHIG	-63.321	302.100	1995.757	2001.046	5.29	53
PERT	-31.802	115.885	1995.834	2001.046	5.21	96
POL2	42.680	74.694	1996.198	2001.046	4.85	80
POTS	52.379	13.066	1995.719	2001.046	5.33	95
REYK	64.139	338.045	1996.121	2001.046	4.93	96
SANT	-33.150	289.331	1995.642	2001.046	5.40	95
SHAO	31.100	121.200	1995.834	2001.046	5.21	83
STJO	47.595	307.322	1995.680	2001.046	5.37	99
THU1	76.537	291.212	1995.642	2001.046	5.40	89
TROM	69.663	18.938	1995.642	2001.046	5.40	45
TSKB	36.106	140.087	1995.642	2001.046	5.40	98
USNO	38.919	282.934	1997.961	2001.046	3.09	97
USUD	36.133	138.362	1995.699	2001.046	5.35	91
VILL	40.444	356.048	1996.217	2001.046	4.83	75
WHIT	60.751	224.778	1996.811	2001.046	4.24	91
WTZR	49.144	12.879	1996.083	2001.046	4.96	98
WUHN	30.532	114.357	1996.849	2001.046	4.20	96
YAKZ	62.031	129.681	1998.229	2001.046	2.82	77
ZECK	43.788	41.565	1998.172	2001.046	2.87	89
ZWEN	55.699	36.759	1995.891	2001.046	5.16	73

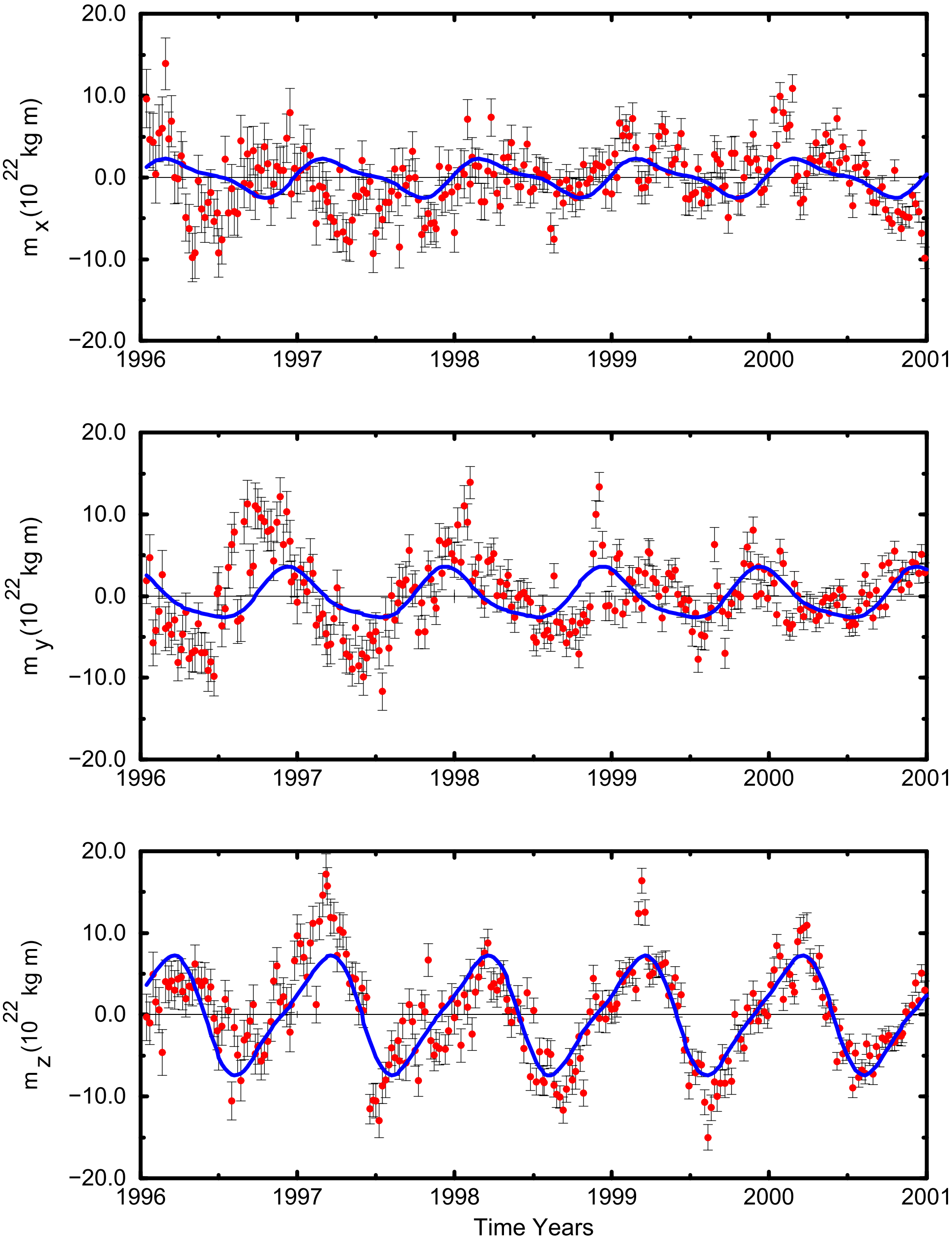

20.0
10.0
0.0
−10.0
−20.0
$m_x(10^{22}$ kg m)
1996
1997
1998
1999
2000
2001
$m_y(10^{22}$ kg m)
$m_z(10^{22}$ kg m)
Time Years

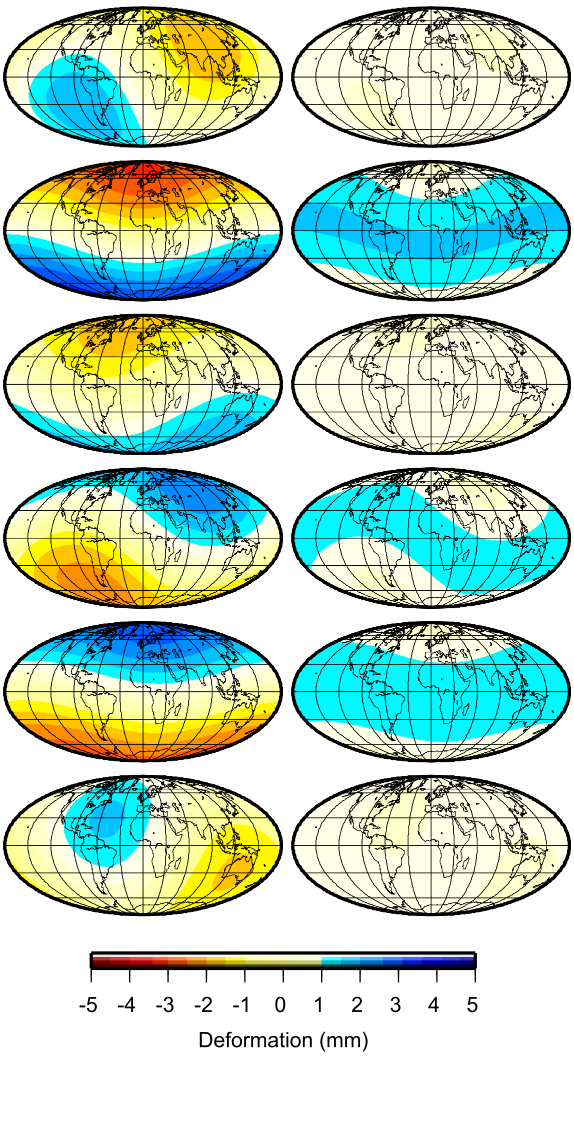
-5 -4 -3 -2 -1 0 1 2 3 4 5
Deformation (mm)

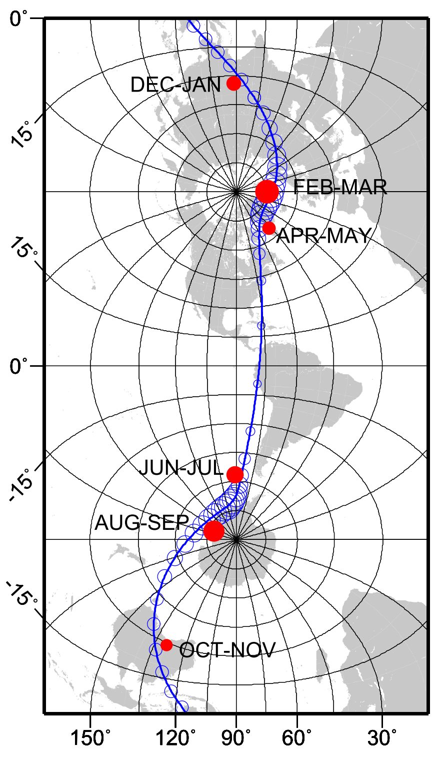

0°
15°
15°
0°
-15°
-15°
DEC-JAN
FEB-MAR
APR-MAY
JUN-JUL
AUG-SEP
OCT-NOV
150°
120°
90°
60°
30°